Polarimetric Characteristics of Tornado Debris Fallout During the May 28 2019 Lawrence/Kansas City, KS Tornado

Erik Y. Wang
Phillips Academy, Andover, Massachusetts

David J. Bodine and James M. Kurdzo
Advanced Radar Research Center, University of Oklahoma, Norman, Oklahoma

James Barham, Chris Bowman, and Pamela Pietrycha
National Weather Forecasting Office, Pleasant Hill, Missouri

ABSTRACT

During the late afternoon and evening on 28 May 2019, an EF-4 tornado affected areas of Northeast Kansas, including the outskirts of Lawrence, KS and the Kansas City metropolitan area. Shortly after EF-3 and EF-4 damage were reported, a large area of lofted debris was evident in the KTWX (Topeka, KS) and KEAX (Kansas City, MO) WSR-88D polarimetric moments. This area of debris drifted northward, resulting in tornadic debris fallout many kilometers north of the tornado. Over 75 km away from the tornado's track, at Kansas City International Airport, falling debris forced crews to shut down the airfield for over 3 hours while debris was cleared from the taxiways and runways. This study presents a statistical analysis of the polarimetric characteristics of the lofted tornadic debris plume, including distributions of the polarimetric moments, distribution of the plume height, and size and directionality of the plume. Each of these analyses is performed on a space-time grid in order to provide temporal context during debris fallout. Differences between the tornadic debris signature and the lofted debris plume are addressed. The data collection and processing scheme is presented in detail, and applicability of the methodology to other cases is discussed.

1. Introduction

Dual-polarization radar enables NEXRAD/WSR-88D radars to receive both horizontal and vertical polarized returns, which provides the capability to differentiate between meteorological and non-meteorological particles (e.g., Zrnic and Ryzhkov 1999). The 28 May 2019 EF4 tornado that affected Lawrence and Kansas City was observed by the National Weather Service's Kansas City WSR-88D dual-polarization radar (KEAX). KEAX provides both Doppler and polarimetric radar variable data in seven to eight-minute sweeps, with a capability of scanning nearby storms up to a 19.5-degree azimuth angle. The tornado produced a substantial amount of damage along its track, and a tornado debris signature (TDS) was evident throughout its lifetime.

Tornadoes loft randomly oriented and variably sized debris, creating a polarimetric signature that is called a tornado debris signature, or TDS (Ryzhkov et al. 2002, 2005; Bluestein et al. 2007; Kumjian and Ryzhkov 2008; Snyder et al. 2010; Palmer et al. 2011; Bodine et al. 2013, 2014). TDSs are characterized by low to high radar reflectivity factor (~40 – 70 dBZ), low co-polar cross-correlation coefficient (ρ_{HV}), and near-zero or sometimes negative differential reflectivity (Z_{DR}). The TDS is also defined to be collocated with the tornadic vortex signature (TVS; Brown et al. 1978). In addition to the TDS, polarimetric radar observations from KEAX also indicate the presence of debris that fell into the forward-flank downdraft (FFD), creating a tornado fallout signature that is produced when winds in stronger, long-lived tornadic environments loft and project large volumes of debris to high altitudes (e.g., Magsig and Snow, 1998; Van Den Broeke et al. 1995). The resulting debris are then dispersed by the storm-scale flow and fall out at low altitudes (Van den Broeke et al. 2015, Bodine et al. 2013). These polarimetric observations offer insight into the transport, shape, size, and positioning of the fallout

signature and its evolution in time. These concentrated regions of debris fallout are characterized by low to moderate horizontal radar reflectivity factor (Z_{HH}), low (near zero) Z_{DR}, and low (below ~0.8) correlation ρ_{HV} (Van Den Broeke et al. 2015).

The KEAX radar provides high-resolution imagery of both the TDS and the tornado fallout signature. The Kansas City tornado produced a large amount of lofted debris, which was ingested into the parent supercell's updraft and fell out downstream. This created a debris plume that had gradually drifted north and east of the primary TDS. There were several local reports of debris falling out of the sky over half an hour after the tornado had dissipated, up to 75 kilometers away from the tornado's path (Weather Forecast Office, 2019). The debris plume also drifted over the Kansas City International Airport, just prior to a ground stop being issued. All departures and arrivals from the airport were suspended for a period of time due to large, dangerous pieces of debris falling out onto the runway (Fig. 1). Falling debris in the vicinity of civilians and planes created the potential for debris ingestion into plane engines, posing a tremendous safety hazard. The debris plume was detected using dual-polarization radar up to 20 min prior to debris falling out over the airport, and thus the detection of the debris plume using polarimetric data may be capable of aiding in making decisions regarding ground stops and rerouting aircraft away from hazardous areas of falling debris in future cases.

Though great improvements have been made in the immediate detection of tornadoes from the TDS, there have been few efforts in quantifying debris fallout and its transport in relation to the TDS over time. Recent studies have explored debris immediately outside the primary TDS, such as debris ejections (Kurdzo et al. 2015; Griffin et al. 2020) as well as debris sedimentation into the storm-scale updraft (Griffin et al. 2020). In addition, Bodine et al. (2013) and Van den Broeke et al. (2015) examined debris fallout in the FFD and rear-flank downdrafts (RFD). Here, we advance this work by examining the temporal evolution of a long-lived debris plume and its application to aviation safety. Specifically, this study examines how polarimetric variables in the fallout signature change over the course of the tornado's life cycle, as well as the relative movement and three-dimensional structure of the fallout signature.

Environmental wind profiles (and associated vertical wind shear) are critical to determining the shape of the fallout signature with height as debris are detrained from the main updraft. The quantification of the polarimetric characteristics in this study may be useful in future investigations of correlations between the longevity of the debris fallout signature or size with real-time tornado intensity.

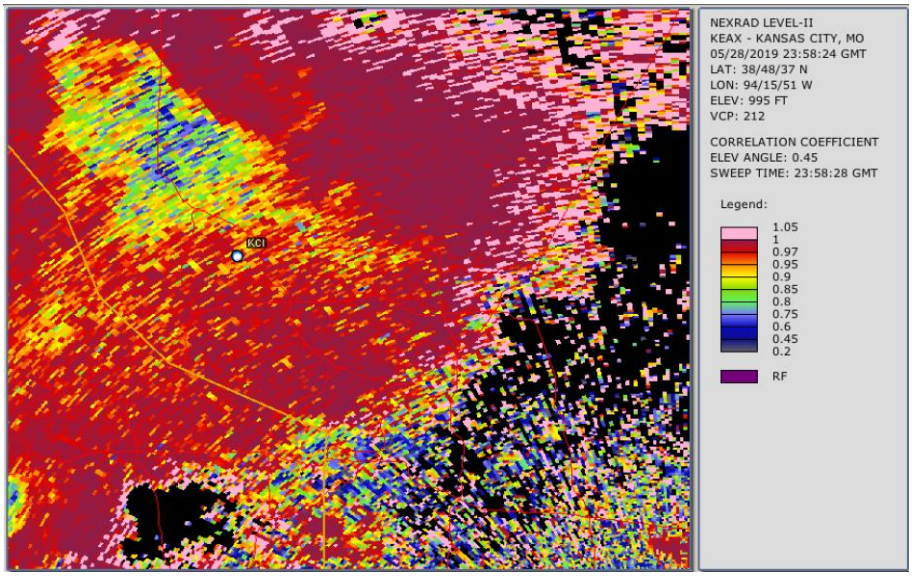

Figure 1: The debris fallout signature is seen to be over the Kansas City International Airport at 23:58 UTC, almost an hour before the airfield closed all the runways due to debris.

2. Event Overview and Tornado Track

During the late afternoon of 28 May 2019, an area of thunderstorms developed in central and eastern Kansas. Between 22:00 – 23:00 UTC, a supercell developed southwest of Lawrence, KS along the warm front and in a region of strong low-level wind shear. The supercell produced a tornado in southwestern Douglas County, KS which continued through to Lawrence, KS and also passed through Linwood, KS. As the tornado traveled northeast, it strengthened to an EF scale rating (McDonald et al. 2004; WSEC 2006) of 3 in Douglas County and reached its maximum strength in southern Leavenworth County, producing EF4-rated damage.

On the National Weather Service's WSR-88D KEAX radar, the first signs of the tornado were detected at around 23:09 UTC (not shown). It was at this time that a small TDS appeared with a defined hook structure in reflectivity factor at horizontal polarization (Z_{HH}) and a rapid inbound/outbound radial velocity differential across the mesocyclone. Although the other cells northeast of this tornadic cell still maintained their strength, only this cell became tornadic.

The National Weather Service's reported tornado track shows the first damage report at 23:05 UTC, which was EF0-rated damage (Fig. 2). The tornado intensified into EF-1 and occasionally EF-2 strength and stayed in between an EF-0 and EF-1 strength for around 10 min. However, the tornado traveled almost 5 km in the span of several minutes. The next recorded debris report, roughly 14 km away and 10 min later at 23:16 UTC, revealed that the tornado had strengthened to an EF-2 rating due to the uplifting and collapse of a barn's roof. From there, the tornado maintained EF-3 damage with occasional bouts of weaker damage indicators until reaching its maximum intensity at around 23:35 UTC. While EF-4 damage was clearly present at that point – the tornado had destroyed multiple one-to-two family residences – the tornado began to gradually weaken until its dissipation at around 00:00 UTC on 29 May 2019. According to the Pleasant Hill, MO NWS survey, the tornado lasted for roughly 55 min, had a pathlength of 51 km and maximum width of 1.6 km, caused 18 injuries, and reached an estimated peak wind speed of 274 km hr^{-1}.

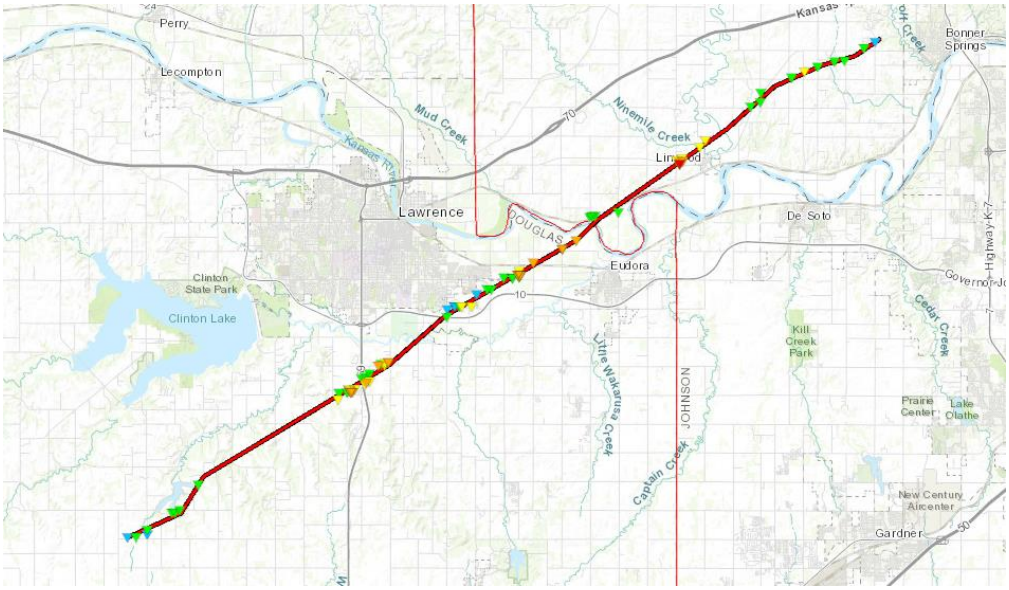

Figure 2: Damage survey of the Lawrence-Linwood Kansas tornado (image courtesy of the Pleasant Hill WFO). Blue, green, yellow, orange, and red triangles show locations of EF-0 to EF-4 damage, respectively.

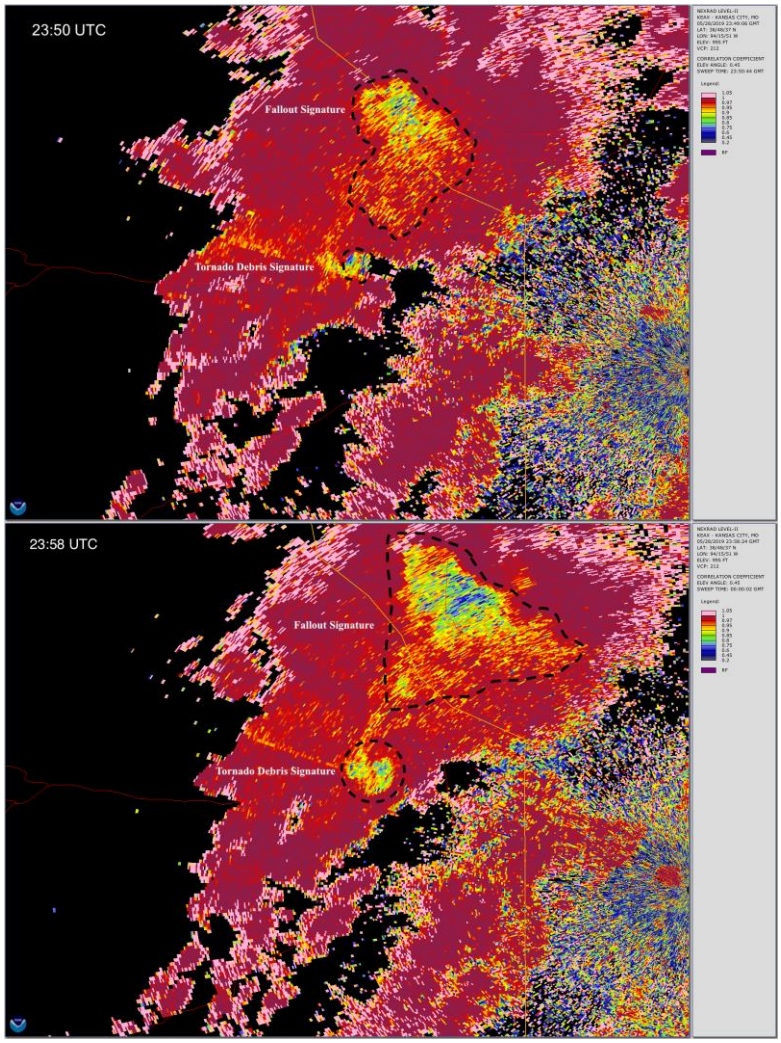

Figure 3: Polarimetric radar image of ρ_{HV} showing the tornado debris signature and tornado fallout signature at 23:50 UTC and 23:58 UTC.

3. Methodology

The transport of tornado debris by sedimentation in the RFD and FFD have been documented and analyzed in numerous studies (e.g., Snow et al. 1995; Magsig and Snow 1998). However, the debris fallout signature – the polarimetric signature that is produced by the ejection of debris from the TDS – has not received significant attention (Van Den Broeke et al. 2015). To address this need, this study will quantify the evolution of the debris fallout signature. The fallout signature's size and time aloft potentially provides substantial insight into the tornado's strength and understanding the processes of debris fallout and its detection using polarimetric radar is critical to the safety of nearby civilians and communities due to potential hazards to aviation.

Polarimetric radar from KEAX is used to investigate the tornado debris signature and debris fallout signature. KEAX operated VCP 212 in SAILS mode without AVSET, providing data from 0.5º to 19.5º as well as high-temporal resolution data at the lowest elevation (~1 – 2 min). For each scan time with a tornado debris fallout signature, a Python lasso tool was developed to manually select the general location of the fallout region and isolate it from other potential areas of low ρ_{HV} such as the primary TDS. Then, to identify the debris fallout signature within the manually identified region, a ρ_{HV} threshold of 0.82 was used, where lower values are flagged as debris. However, in contrast to detection of the primary

TDS, a reflectivity threshold is not used because the debris fallout contains much lower values of radar reflectivity factor. Similar behavior was noted for storm-scale debris sources in Griffin et al. (2020), who used a 10-dBZ threshold for debris falling out on the periphery of the storm-scale updraft or lofted along the rear-flank gust front.

Once the debris fallout signatures are identified for each time, a variety of statistics are computed to evaluate the properties and evolution of the debris fallout signature. Detailed information like the values of polarimetric variables, vertical and areal extent, 3-dimensional position, and appearance and disappearance times were recorded for each available radar elevation angle and scan. This collection of data allowed for a comparison between fallout signature characteristics at different positions and times, and thus created an analysis opportunity of the fallout signature's evolution over time (Figs. 4 and 5).

4. Analysis of the Fallout Signature

a. Distribution

The KEAX WSR-88D provides extensive coverage of the tornado's debris fallout signature throughout the tornado's life cycle. Statistical distributions of ρ_{HV}, Z_{HH}, and Z_{DR} were each plotted. The values of these polarimetric variables were collected from each of the radar scans at each of the available radar elevations. Values of the fallout signature were only collected if a noticeable fallout signature was present; in other words, very dispersed and scattered debris particles that had not collected into a substantial fallout signature were not considered a fallout signature and thus the polarimetric variables for such debris were not recorded.

The three histograms show ρ_{HV}, Z_{HH}, and Z_{DR} within the debris fallout signature (Fig. 3). ρ_{HV} has a higher concentration of higher values, suggesting smaller or less-concentrated debris than the primary TDS. ρ_{HV} values of greater than 0.8 are of the highest frequency, and the lowest ρ_{HV} values have the lowest frequency. The reflectivity plot shows a much-wider distribution and lower mean due to the broad dispersion of debris, which is counter to more narrow distributions of higher values typically seen in the primary TDS. Z_{DR} also has a near-zero mean, whereas the mean is sometimes negative in the primary TDS from this tornado, suggesting that the debris fallout is randomly oriented (Bodine et al. 2011, Griffin et al. 2017).

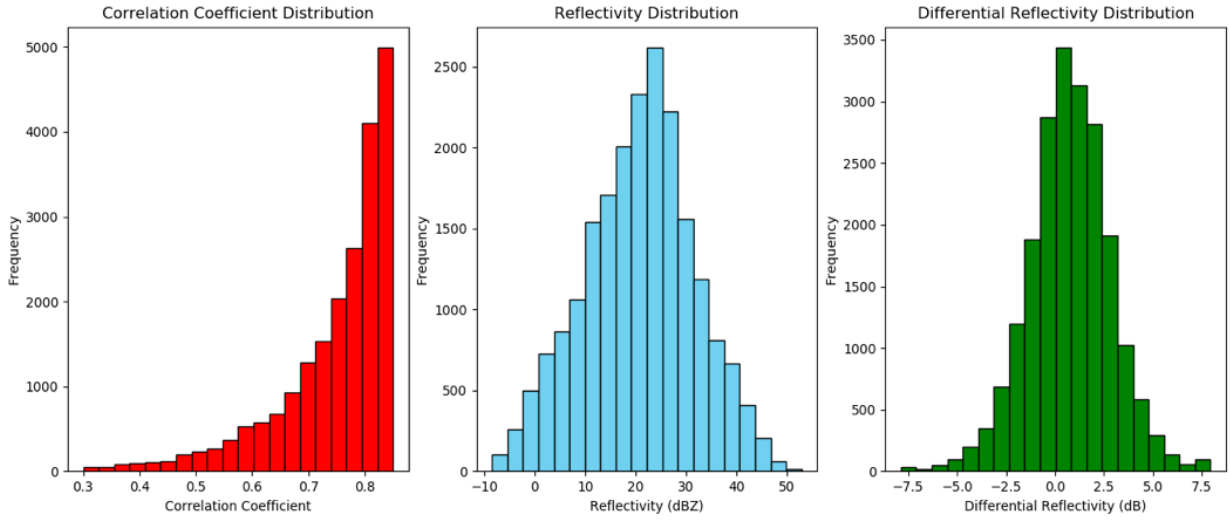

Figure 3: Histograms of correlation coefficient, reflectivity, and differential reflectivity in the debris fallout plume.

b. Fallout Area

The official start time of the tornado as reported by the NWS is at 23:05 UTC on 28 May 2019. However, despite official sightings of the tornado at 23:05 UTC, its wind speed and intensity were low, giving the tornado an EF-0 damage rating. Thus, significant amounts of debris only began to collect into a recognizable fallout signature at around 23:41 UTC despite there being large debris particles aloft at earlier times. Fig. 4b illustrates the total area of the debris across all elevations, starting at 23:27 UTC. Over time, there is a significant increase in fallout area at low elevations, particularly between 1 – 2 km in altitude. The debris aloft between 1 – 2, 2 – 3 km, and 3 – 4 km are substantial compared to other elevations, with total area of debris across elevations of approximately 125 km^2 and more than 30 km^2 of debris aloft between 1 – 2 and 2 – 3 km in altitude at 23:58 UTC. The higher elevation scans at 00:05 UTC reveal a significant decrease in total fallout area: the total area of fallout debris decreases by more than 40% from 23:58 UTC to 00:05 UTC between 3 – 4 km in altitude, and the area of debris between 2 – 3 km in altitude decreases by almost 20%. However, debris fallout at 1 km continues to increase as debris fall toward the surface. The tornado's dissipation occurred at 00:00 UTC based on the NWS damage survey, and the TDS disappeared at 00:05 UTC, which would have abated the ejection of debris aloft and its sedimentation into the FFD. Nonetheless, the areal extent of the fallout signature continues to expand after tornado dissipation as debris disperse farther downwind.

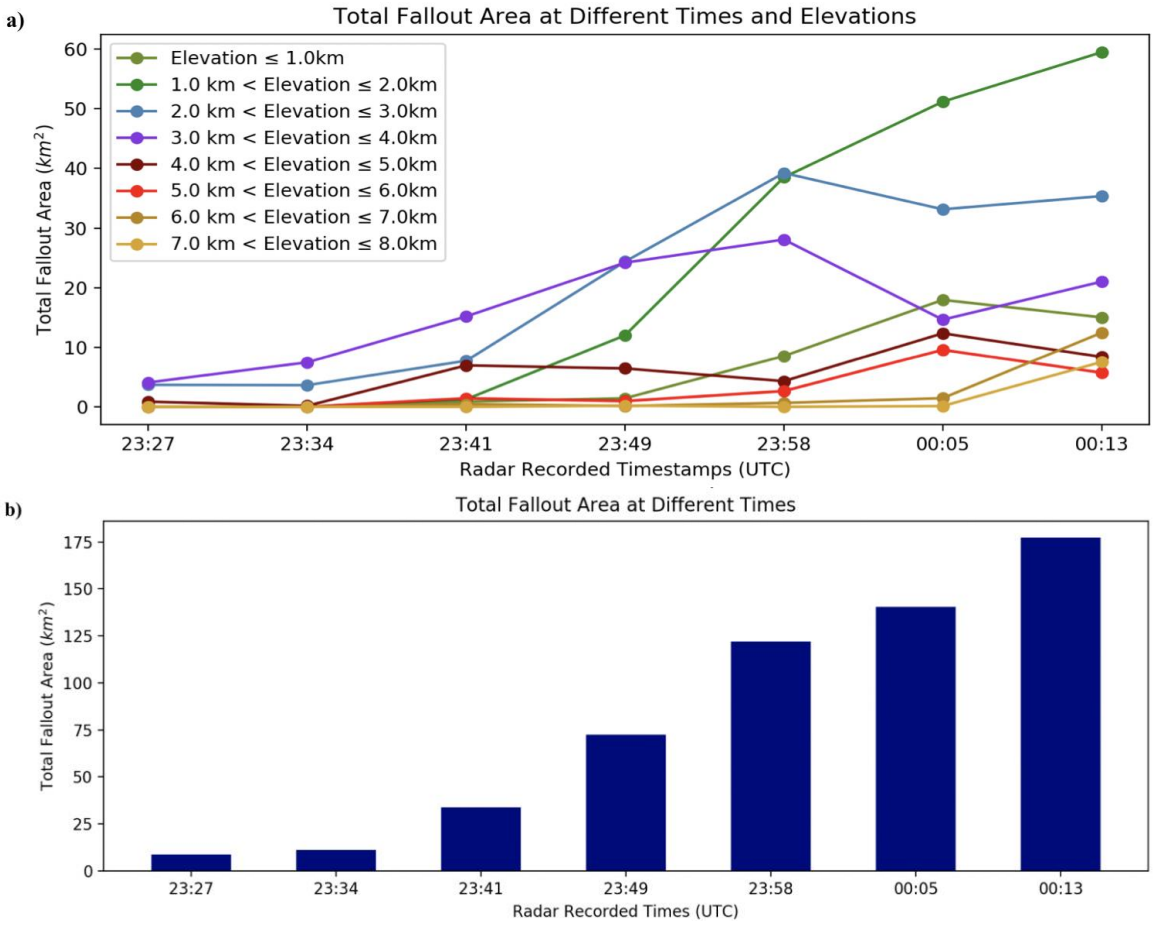

Figure 4: Different timestamps ranging from 28 May 2019 at 23:27 UTC to 29 May 2019 at 00:13 UTC, showing the progression in total fallout area in km^2, filtered out over 1-km elevation groupings.

c. Vertical Structure

As seen in Fig. 5, there is a substantial change in the fallout signature's position over height and over time. In respect to west-east distance from the radar, the debris is generally the furthest away from the radar at lower elevations than higher elevations at earlier times. 23:41 and 23:49 UTC in Fig. 5a shows the generally decreasing trend of the fallout signature's longitudinal distance from the radar. At later times, though, the highest elevation scan shows debris that is the farthest west from the radar despite having been the closest in comparison to lower elevations at earlier times.

The correlation between latitudinal distance from the radar, debris altitude, and time is different from the associated relationship with longitudinal distance. The debris held in the highest elevation scan are consistently the closest to the radar at each of the times from 23:41 to 00:13 UTC. Instead, debris held in the lowest sweep, at a 0.9° tilt, is the closest to the radar in terms of latitudinal distance at 23:41 and 23:49 UTC, but eventually becomes the furthest away from the radar at the rest of the times. Like the debris plotted in Fig. 5a, the debris in the first three elevation tilts (0.9°, 1.3°, and 1.9°), are relatively close in terms of distance from the radar.

The vertical structure and "shape" of the fallout signature is likely caused by the vertical wind profile and its speed and directional shear. So, the higher altitudes in which the debris is seen to be located further away from the radar at later times may correspond to a strong jet advecting the debris away from the updraft. The debris that generally shifts northward and westward as altitude decreases and as time increases suggests that fallout signature's non-linear vertical structure is advected downstream through southwesterly flow aloft and southerly flow near the surface.

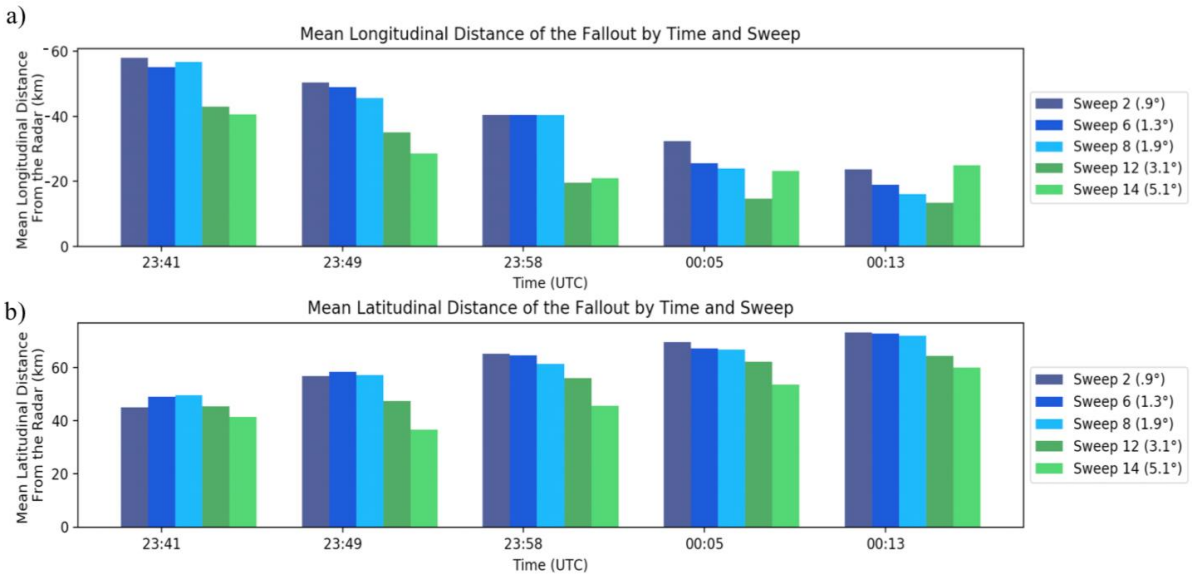

Figure 5: Average longitudinal and latitudinal distance from the radar, sorted by sweep (radar elevation angle) and time from the 28th evening to the 29th early morning. Fig. 5a shows east-west distance from the radar; Fig. 5b shows north-south distance from the radar.

5. Impact of Debris Fallout on Airport Operations

After the NWS issued a tornado warning at 23:51 UTC, the Kansas City International Airport Traffic Control Tower (ATCT) promptly evacuated, according to airport operations. At around 00:01 UTC, the airport issued a public announcement in all of the passenger terminals to take shelter as the airport had been notified that a possible tornado was heading toward KCI. The tornado warning was in place until 00:34 UTC, when the NWS cancelled the tornado warning since the tornado had dissipated. Shortly after receiving the all clear from the NWS, KCI closed the airfield at 00:50 UTC due to debris on

runways and taxiways. The airport's field maintenance crews called for sweeping, and up to three broom trucks swept the runways for debris. Because of the hazardous conditions arising from the falling debris, airport operations suspended aircraft takeoffs and landings for more than four hours. Before the runways were closed by the airport, two commercial flights landed after the debris fallout signature was observed over the airport, so debris may have already fallen on or near the runways while the two aircraft were landing. This clearly demonstrated a dangerous situation for these flights and could potentially be avoided in future cases with proper warning.

According to the ATCT, their radar system was unable to detect the tornado's debris. Despite the debris having traveled up to 26 miles from the tornado to the airport, there were several, large chunks of debris that could have been extremely hazardous to airport staff, airplanes, and passengers. If the ATCT had known that there was a high probability of debris falling on the airfield, air traffic would most likely have put inbound aircraft into a holding pattern or diverted them to nearby airports to prevent dangerous landing conditions. Furthermore, there was no way of determining the exact time the debris had fallen onto the airfield, despite having been able to quickly recover the debris. Though the runways were first closed at 00:50 UTC when the airfield inspection first noted debris on the runways, the first evidence of debris falling out at the airport site was spotted almost an hour before at 23:58 (Fig. 7). Several of the debris were of considerable weight and size, with the heaviest being the lid of a typical pick-up truck's toolbox and the largest being a 3.5' by 8' sheet of corrugated steel. Luckily, the airport sustained no aircraft damage or injuries resulting from the falling debris.

Figure 7: Debris collected by the Kansas City International Airport's ground staff and the National Weather Service on the airport's runway showing the various sizes of the objects.

6. Conclusion and Future Work:

The 28 May 2019 EF-4 tornado case was analyzed to study a debris fallout signature and evaluate its potential use for aviation safety following an airport closure due to falling debris on the runway. Unlike the TDS, the tornado debris fallout signature has not been as thoroughly studied. Careful examination of the fallout signature reveals rapid growth in the volume of debris. This study analyzes the debris fallout signature on a space-time grid to identify the distribution of the polarimetric characteristics, the size and directionality of the debris plume, the transport of the plume in relation to the radar over time, and the areal extent of the debris. The formation of the debris fallout signature can be attributed to the lofting of debris from the main tornado vortex, followed by subsequent dispersion by the environmental flow aloft.

As the first known case of tornado debris impacting airport operations, it is evident that a method of predicting or detecting the fallout debris plume ahead of time to divert aircraft and cancel flights would have been extremely beneficial to air traffic control and for the safety of passengers. From an aviation safety standpoint, the debris plume was located in areas of light precipitation on the northern edge of the

supercell and in non-precipitating regions ahead of the supercell, both regions that commercial aircraft would not necessarily avoid from available observations (e.g., airborne radar data or visual cues). Thus, polarimetric radar data can help identify and track plumes of debris that pose a hazardous to aircraft in all phases of flight. Although the probability of debris impacting an aircraft are relatively small, the consequences are potentially severe if it causes damage to aircraft engines in any phase of flight, or to tires during take-off or landing.

In the future, an extensive number of social media reports of debris fallout (e.g., Knox et al. 2013) will be categorized using GIS mapping for comparisons to the polarimetric fallout signature. In some cases, the debris contained sufficient information to determine their source locations. Such debris included a greenhouse in Linwood, KS, which comprised some of the debris found at the airport. Trajectory analyses will be conducted to explore the three-dimensional path of the debris as well as to better understand the sedimentation process. Finally, the relationship between along-path damage, the TDS, and the fallout signature from this case will be investigated. Once the analysis of the 28 May 2019 case is completed, a more extensive climatology of debris fallout signatures from a large pool of strong tornadoes will be undertaken.

Acknowledgements. David Bodine is supported by the National Science Foundation (NSF) AGS-1823478. The authors greatly appreciate the Kansas City International Airport for providing valuable information into the airport operations during the debris fallout onto the runways. NEXRAD data can accessed from https://data.nodc.noaa.gov/cgi-bin/iso?id=gov.noaa.ncdc:C00345#.

REFERENCES

Bluestein, H. B., C. C. Weiss, and A. L. Pazmany, 2004: The vertical structure of a tornado near Happy, Texas, on 5 May 2002: High-resolution, mobile, W-band, Doppler radar observations. *Mon. Wea. Rev.*, **132**, 2325–2337.

Bodine, D., M. R. Kumjian, A. J. Smith, R. D. Palmer A. V. Ryzhkov, and P. L. Heinselman, 2011: High resolution polarimetric observations of an EF-4 tornado on 10 May 2010 from OU-PRIME. 35th Conf. on Radar Meteorology, Pittsburgh, PA, Amer. Metor. Soc.

———, M. R. Kumjian, R. D. Palmer, P. L. Heinselman, and A. V. Ryzhkov, 2013: Tornado damage estimation using polarimetric radar. *Wea. Forecasting*, 28, 139–158.

———, R. D. Palmer, and G. Zhang, 2014: Dual-wavelength polarimetric radar analyses of tornadic debris. *J. Appl. Meteor. Climatol*., 53, 242–261.

Brown, R. A., L. R. Lemon, and D. W. Burgess, 1978: Tornado detection by pulsed Doppler radar. *Mon. Wea. Rev*., 106, 29–38.

———, B. A. Flickinger, E. Forren, D. M. Schultz, D. Sirmans, P. L. Spencer, V. T. Wood, and C. L. Ziegler, 2005a: Improved detection of severe storms using experimental fine-resolution WSR-88D measurements. *Wea. Forecasting*, 20, 3–14.

Griffin, C. B., D. J. Bodine, and R. D. Palmer, 2017: Kinematic and polarimetric radar observations of the 10 May 2010, Moore-Choctaw, Oklahoma, tornadic debris signature. *Mon. Wea. Rev*., 145, 2723-2741.

———, 2020: Polarimetric radar observations of simultaneous tornadoes on 10 May 2010 near Norman, Oklahoma. *Mon. Wea. Rev.,* 148**,** 477 – 497.

Helmus, J.J. & Collis, S.M., (2016). The Python ARM Radar Toolkit (Py-ART), a Library for Working with Weather Radar Data in the Python Programming Language. *Journal of Open Research Software*. 4(1), p.e25. DOI: http://doi.org/10.5334/jors.119

Knox, J.A., J.A. Rackley, A.W. Black, V.A. Gensini, M. Butler, C. Dunn, and S. Brustad. "Tornado Debris Characteristics and Trajectories During the 27 April 2011 Super Outbreak as Determined Using Social Media Data." *Bulletin of the American Meteorological Society*, 94 (2013, 9): 1371-1380.

Kumjian, M. R., and A. V. Ryzhkov, 2008: Polarimetric signatures in supercell thunderstorms. *J. Appl. Meteor. Climatol*., 47, 1940–1961.

Kurdzo, J. M., D. J. Bodine, B. L. Cheong, and R. D. Palmer, 2015: High-temporal resolution polarimetric X-band Doppler radar observations of the 20 May 2013 Moore, Oklahoma, tornado. *Mon. Wea. Rev.*, **143**, 2711–2735.

Magsig, M. A., and J. T. Snow, 1998: Long-distance debris transport by tornadic thunderstorms. Part I: The 7 May 1995 supercell thunderstorm. *Mon. Wea. Rev.,* 126, 1430–1449.

May, R. M., Arms, S. C., Marsh, P., Bruning, E., Leeman, J. R., Goebbert, K., Thielen, J. E., and Bruick, Z., 2020: MetPy: A Python Package for Meteorological Data. Version 0.12.0, Unidata, Accessed 06 January 2020. [Available online at https://github.com/Unidata/MetPy.] doi:10.5065/D6WW7G29.

McDonald, J. R., G. S. Forbes, and T. P. Marshall, 2004: The en- hanced Fujita (EF) scale. Preprints, 22nd Conf. on Severe Local Storms, Hyannis, MA, Amer. Meteor. Soc., 3B.2. [Available online at http://ams.confex.com/ams/pdfpapers/81090.pdf.]

Palmer, R. D., and Coauthors, 2011: The 10 May 2010 tornado outbreak in central Oklahoma: Potential for new science with high-resolution polarimetric radar. *Bull. Amer. Meteor. Soc.*, 92, 871–891.

Snow, J. T., A. L. Wyatt, A. K. McCarthy, and E. K. Bishop, 1995: Fallout of debris from tornadic thunderstorms: A historical perspective and two examples from VORTEX. *Bull. Amer. Meteor. Soc.*, 76, 1777–1790.

Van Den Broeke, M. S., 2015: Polarimetric tornadic debris signature variability and debris fallout signatures. *J. Appl. Meteor. Climatol.*, 54, 2389–2405.

Weather Forecast Office (Ed.). (2019). 28 May 2019 Tornadoes. Retrieved January 11, 2020, from National Weather Service website: https://www.weather.gov/eax/28May2019_Tornadoes.

Zrnić, D. S., and A. V. Ryzhkov, 1999: Polarimetry for weather surveillance radars. *Bull. Amer. Meteor. Soc.*, 80, 389–406.